

# Near infrared absorption and room temperature photovoltaic response in AlN/GaN superlattices grown by metal-organic vapor-phase epitaxy

E. Baumann, F. R. Giorgetta,<sup>a)</sup> and D. Hofstetter  
*University of Neuchâtel, 1 Abram-Louis Breguet, Neuchâtel CH 2000, Switzerland*

S. Golka, W. Schrenk, and G. Strasser  
*Institut für Festkörperphysik and Zentrum für Mikro- und Nanostrukturen, Technische Universität Wien, 1040 Vienna, Austria*

L. Kirste  
*Fraunhofer-Institute of Applied Solid State Physics, Tullastrasse 72, Freiburg D 79108, Germany*

S. Nicolay, E. Feltin, J. F. Carlin, and N. Grandjean  
*Institute of Quantum Electronics and Photonics, Ecole Polytechnique Fédérale de Lausanne (EPFL), CH-1015 Lausanne, Switzerland*

We report on intersubband absorption of near infrared radiation in AlN/GaN superlattice structures grown by metal-organic vapor-phase epitaxy. A good correlation between well thickness and absorption peak energy was obtained. One sample shows a photovoltaic signal which overlaps well with the corresponding absorption curve at around  $1.5 \mu\text{m}$  (830 meV), a common wavelength in optical fiber telecommunication systems. This photovoltaic signal is strongest at temperatures around 75 K and persists up to room temperature. The frequency response of this sample was measured with a modulated  $1.5 \mu\text{m}$  laser diode. The amplitude of the response was highest for a frequency of 36 kHz.

Due to its large conduction band discontinuity, the AlN/GaN material system is considered as a promising candidate for fast quantum well infrared photodetectors (QWIPs) for telecommunication wavelengths around  $1.55 \mu\text{m}$ .<sup>1</sup> Up to now, photovoltaic and photoconductive signals were demonstrated in AlN/GaN superlattices grown by molecular beam epitaxy (MBE) only.<sup>2-4</sup> Today, most nitride based commercial optoelectronic devices are grown by metal-organic vapor-phase epitaxy (MOVPE).<sup>5</sup> However, the higher temperature during MOVPE is believed to lead to more gradual interfaces than MBE. As quantum well and barrier layer thicknesses on the order of 1–2 nm are required to obtain near infrared intersubband (ISB) absorption with III-nitrides, MOVPE of such devices is more challenging than MBE. Accordingly, the shortest measured ISB absorption wavelength in MOVPE grown material was so far  $2.4 \mu\text{m}$  in an  $\text{Al}_{0.6}\text{Ga}_{0.4}\text{N}/\text{GaN}$  superlattice;<sup>6,7</sup> and a large linewidth broadening indicated severe thickness fluctuations and interface roughness.

In this letter, we therefore present AlN/GaN samples, which were fabricated by an optimized MOVPE process. The material was then characterized by rapid scan transmission, electromodulated absorption (EMA), and photovoltaic response (PV) measurements. Three MOVPE grown AlN/GaN superlattice samples were investigated (see Table I). Growth was carried out in an AIXTRON 200/4 RF-S MOVPE reactor on 2 in. *c*-plane sapphire substrates. The active region was deposited at low temperature (885–935 °C) on a  $2 \mu\text{m}$  GaN buffer layer grown at 1075 °C. The GaN well thicknesses vary between 1 and 1.8 nm to have access to a large range of transition energies. Samples A and B were covered with a 30 nm thick AlN cap.

In the case of sample C, In was used as a surfactant in the barriers in order to improve the surface morphology. Note that this process results in a small amount of In incorporation (2%).<sup>8</sup> In all cases, the wells are Si doped at nominally  $5 \times 10^{18} \text{cm}^{-3}$  while the barriers are undoped. Due to the tensile strain of the superlattices, samples A and B (30 periods) show cracks. Sample C (ten periods), on the other hand, has a lower average Al content, and therefore exhibits no cracks.

For absorption measurements, all samples were polished in multipass geometry using two 45° wedges, followed by the evaporation of two Ohmic contact stripes. For samples A and B, two Ti/Al/Ti/Au (15 nm/200 nm/15 nm/400 nm) Ohmic stripes of  $0.5 \times 6 \text{mm}^2$  were annealed at 790 °C for 60 s and a Schottky-like Ti/Au (10 nm/400 nm) contact was evaporated between the two Ohmic stripes. As sample C does not have an insulating AlN cap, two Ti/Au (10 nm/400 nm) contact stripes served as Ohmic contacts. In order to obtain a Schottky contact in between, a similar Ti/Au (10 nm/400 nm) contact stripe was evaporated on top of a 100 nm thick  $\text{Si}_3\text{N}_4$  layer grown by plasma enhanced chemical vapor deposition. In a second process run, sample A was processed in 400 nm high square mesa structures with a side length of  $400 \mu\text{m}$ . Ti/Au contacts were sputtered on top of the mesas. For the characterization, the samples were mounted into a liquid He flow cryostat and illuminated by

TABLE I. Sample description.

Sample	Cap	Well/barrier thickness (nm)	Number of periods	Barrier
A	30 nm AlN	1/5	30	AlN
B	30 nm AlN	1.6/2	30	AlN
C	No cap	1.8/2	10	$\text{Al}_{0.98}\text{In}_{0.02}\text{N}$

<sup>a)</sup>Electronic mail: fabrizio.giorgetta@unine.ch

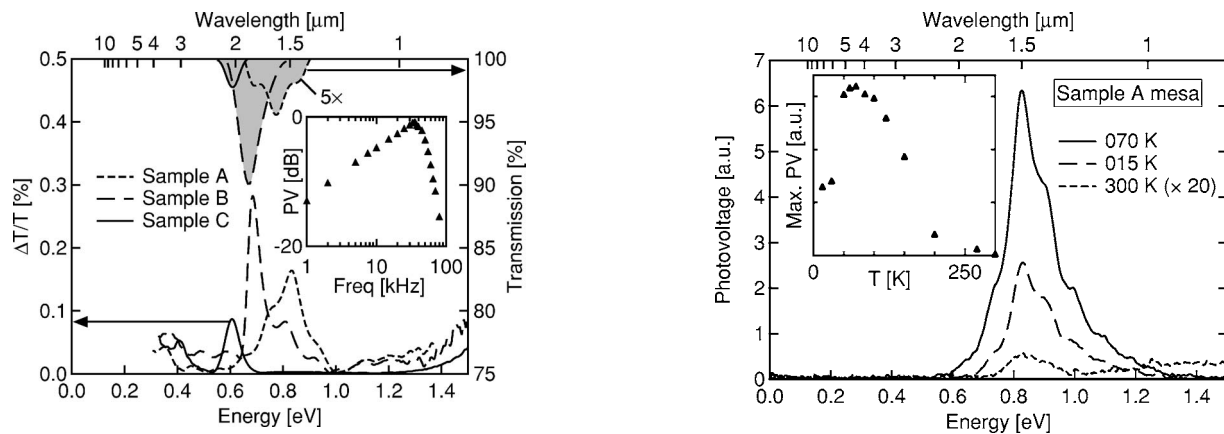


FIG. 1. Rapid scan transmission and EMA of samples A, B, and C. The inset shows the normalized PV frequency response of sample A (stripe) at 75 K.

the white light source of a Fourier transform infrared (FTIR) spectrometer.

As stated before, absorption was measured in the usual rapid scan configuration and by EMA, a lock-in/step scan detection technique allowing us to measure absorption changes on the order of 0.1%.<sup>9</sup> For the latter, a voltage square wave with a base line of 0 V and an amplitude of  $-2$  V at a frequency of 13 kHz and 50% duty cycle was applied between the Schottky and the Ohmic contact of the sample. It periodically reduces the carrier density in the wells closest to the Schottky contact and thus modulates the transmission of the FTIR light beam. The modulated signal of the FTIR mercury cadmium telluride detector is amplified by a lock-in amplifier synchronized with the voltage square wave and fed back into the FTIR, whose mirror is slowly stepped at intervals longer than the amplifiers integration time. This measurement ( $\Delta T$ ) is normalized with a rapid scan FTIR measurement of the sample ( $T$ ), yielding the differential transmission  $\Delta T/T$ . The latter quantity, which is proportional to the absorbance, is used to label our EMA measurements.

In Fig. 1 the rapid scan transmission and EMA in TM polarization are depicted. The two techniques are in very good agreement. The peak energy  $E$  is highest for sample A (834 meV/1.49  $\mu\text{m}$ ), followed by sample B (685 meV/1.81  $\mu\text{m}$ ) and C (608 meV/2.04  $\mu\text{m}$ ). This behavior correlates in the expected way with the nominal well thicknesses of 1 nm (A), 1.6 nm (B), and 1.8 nm (C). The full width at half maximum (FWHM)  $\Delta E$  and the respective quality factors  $E/\Delta E$  of the absorption curves are 145 meV and 5.75 (A), 78 meV and 8.78 (B), and 61 meV and 9.97 (C). In a 4 ML well (A), a 1 ML interfacial roughness leads to more severe linewidth broadening and thus a lower quality factor than in a 7 monolayer (ML) well (C). The different strengths of the EMA are caused by both the varying insulator thickness between the metal contact and the active region (30 nm AlN for samples A and B and 100 nm  $\text{Si}_3\text{N}_4$  for sample C) and the decreasing oscillator strength for thinner wells. An estimation based on Fermi's golden rule<sup>10</sup> and the measured EMA leads to the conclusion that only the topmost wells contribute to the absorption. The different absorption strengths of the rapid scan measurements are caused by the varying number of wells (A and B: 30, C: 10) and again the oscillator strength.

The broad absorption of sample A is due to several reasons. First, the thin wells of sample A cause the first excited

state to be close to the continuum. Second, transmission electron microscopy measurements show a quantum well thickness variation along the growth direction. Third, a high-resolution x-ray diffractometry indicates a gradual relaxation of the superlattice, leading to a gradual change of the band offset.<sup>11</sup> As the first excited state lies close to the continuum, a change in the band offset will critically affect the absorption spectrum. In the other two samples, which have a bound transition, the changing band offset has a much smaller influence on the transition energy.

The frequency response of the stripe process of sample A was measured by illuminating the Schottky contact with a sinusoidally modulated 1.5  $\mu\text{m}$  laser diode and measuring the voltage between this contact and a reference Ohmic contact. The inset of Fig. 1 shows the measured normalized amplitude of this sample's PV signal for different laser modulation frequencies at 75 K. This PV frequency response peaks at 36 kHz, which is valid for the entire temperature range between 15 and 150 K (not shown in the figure). Considering the fast ISB relaxation times of GaN, which are as short as 160 fs,<sup>1</sup> much higher modulation speeds are expected. In addition, the peak frequency of the PV signal is identical for the mesa process with a contact area of  $400 \times 400 \mu\text{m}^2$  and the stripe process with a contact area of  $0.5 \times 6 \text{ mm}^2$ . Therefore, the PV frequency response cannot be explained with contact parasitics. The most likely explanation is the occurrence of a tunneling process involving defect levels in the AlN barrier layers, which makes it extremely slow.

PV measurements were also carried out for the processed mesa structure of sample A. The measured voltage between the illuminated mesa and a reference ground was amplified and fed back into the FTIR. This PV signal was analyzed between 10 K and room temperature, as shown in Fig. 2. The PV signal, which peaks at 842 meV (1.47  $\mu\text{m}$ ), increases rapidly between 30 and 50 K, is maximal around 75 K, and diminishes again towards higher temperatures, as seen in the inset of Fig. 1. At room temperature, where the ISB PV is still visible, a broad signal around 1.4 eV appears. We believe that this signal is caused by defects in the GaN well material;<sup>12</sup> other than that, the signal shape does not change with temperature. Calculations of the temperature-induced mobility variation in GaN for a dislocation density of  $5 \times 10^{10} \text{ cm}^{-2}$  and a carrier density of  $5 \times 10^{19} \text{ cm}^{-3}$  (as opposed to  $5 \times 10^{18} \text{ cm}^{-3}$  in our samples) show a maximum

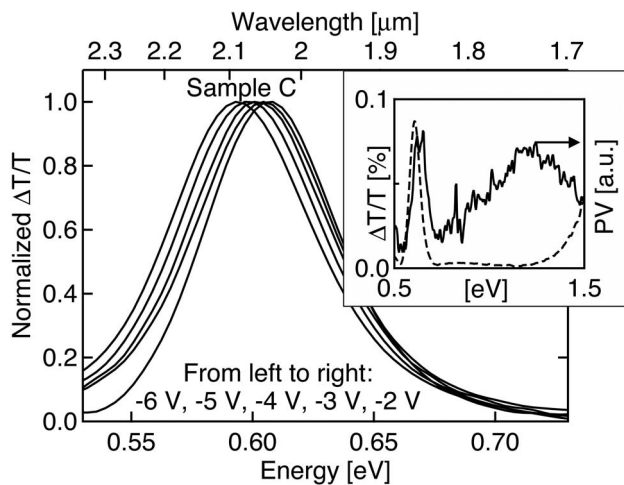


FIG. 3. Normalized EMA of sample C as function of modulation voltage amplitude. The inset shows the PV of sample C at 15 K (bold line) and the EMA for  $-2$  V (dashed line).

around 80 K,<sup>13</sup> which could explain the maximal PV signal amplitude at 75 K. A small blueshift of 8 meV is observed for the PV relative to the absorption. As explained in our earlier publications, this is attributed to the higher tunneling probability at the upper edge of the miniband formed by the first excited states of the superlattice.

In Fig. 3 the normalized electromodulated absorption of sample C for different negative voltage amplitudes is shown. A negative voltage amplitude decreases the internal piezo and spontaneous electrical fields in AlN/GaN heterostructures and hence weakens the Stark effect. This results in a redshift of the ISB transition energy.<sup>14</sup> The measured shift is linear with a slope of  $-3.7$  meV/V for bias amplitudes between  $-2$  and  $-6$  V; for positive bias amplitudes no shift was observed, most likely due to the increased leakage current of the Schottky contacts which resulted in a less efficient modulation of the electric field in the active region. For calculating the above shift, the common second order perturbation method is not appropriate as it relies on weak fields. Since the piezo- and pyroelectrical fields in our structures are as high as 5.7 MV/cm, we had to use a variational calculation to obtain an estimate of the external field in the wells.<sup>14</sup> The equation describing the shift is then given by

$$\Delta E_1 = -\frac{|q|FL}{2} + \left(\frac{3}{2}\right)^{5/3} \left(\frac{q^2 F^2 \hbar^2}{m^*}\right)^{1/3}, \quad (1)$$

where  $\Delta E_1$  is the shift of the ground state,  $q$  the elementary charge,  $F$  the applied field,  $L$  the well thickness, and  $m^*$  the effective electron mass of GaN. When starting from a “zero-external-field” configuration ( $F_{\text{int}} = 5.7$  MV/cm), an external field of  $F_{\text{ext}} = 172$  kV/cm opposite to the internal field must be applied to result in a Stark shift of 3.7 meV towards lower energies. Assuming further that only the top five wells with a total thickness of  $t = 19$  nm (including barriers) contribute to the absorption as stated above, a total voltage drop of  $V = F_{\text{ext}}t = 300$  mV is needed. Considering finally that a substantial fraction of the applied field drops across the  $\text{Si}_3\text{N}_4$  layer, an external voltage amplitude difference of 1 V seems to be a reasonable value to change the total electric field in the active region in the desired way.

This field-dependent shift of the EMA was best seen in sample C. Comparing the  $IV$  characteristics between the

Schottky and the Ohmic contacts of the three samples, sample C (no cap layer, 100 nm  $\text{Si}_3\text{N}_4$ ) has the lowest leakage current of  $\sim 0.1$  nA in reverse direction. This leads to the conclusion that only samples with a low leakage current will allow us to build up a sufficiently high electric field in the active region to observe a decrease of the absorption peak energy.

In the same experiment setup as for the PV measurement for sample A, a weak PV signal at 15 K was measured for sample C. The inset of Fig. 3 shows the PV signal in comparison with the electromodulated absorption of sample C measured with a modulation voltage amplitude of  $-2$  V. Again a blueshift for the PV relative to the absorption is observed. The broad peak around 1.2 eV is again believed to be due to defects. The difference in the PV signal strength of sample A and C is among others due to the different number of periods.

In conclusion, we have measured ISB absorption for three different MOVPE grown AlN/GaN superlattices up to 834 meV (1.49  $\mu\text{m}$ ) and shown that the peak absorption energy increases with decreasing well width. Two samples show PV signals which agree well with the absorption maxima. For the sample whose absorption was at 834 meV (1.49  $\mu\text{m}$ ), a PV signal at 841 meV (1.47  $\mu\text{m}$ ) was observed up to room temperature. The frequency response of the PV signal peaks at 36 kHz, leaving much room for future improvement of nitride ISB light detecting devices.

The authors thank the Professorship Program and the National Center of Competence in Research “Quantum Photonics” of the Swiss National Science Foundation, the Sandoz Family Foundation, as well as the European project NITWAVE (Contract No. 004170) for their generous financial support. Furthermore, the authors thank S. Dunand (IMT, University of Neuchâtel, Switzerland) for technical assistance, as well as P. Stadelmann and C. Tobler (CIME/EPFL) for transmission electron microscopy characterization.

<sup>1</sup>J. D. Heber, C. Gmachl, H. M. Ng, and A. Y. Cho, *Appl. Phys. Lett.* **81**, 1237 (2002).

<sup>2</sup>D. Hofstetter, S.-S. Schad, H. Wu, W. J. Schaff, and L. F. Eastman, *Appl. Phys. Lett.* **83**, 572 (2003).

<sup>3</sup>E. Baumann, F. R. Giorgetta, D. Hofstetter, H. Wu, W. J. Schaff, L. F. Eastman, and L. Kirste, *Appl. Phys. Lett.* **86**, 032110 (2005).

<sup>4</sup>E. Baumann, F. R. Giorgetta, D. Hofstetter, H. Lu, X. Chen, W. J. Schaff, L. F. Eastman, S. Golka, W. Schrenk, and G. Strasser, *Appl. Phys. Lett.* **87**, 191102 (2005).

<sup>5</sup>S. Nakamura, G. Fasol, and S. J. Pearton, *The Blue Laser Diode: The Complete Story* (Springer, New York, 1997).

<sup>6</sup>I. Waki, C. Kumtornkittikul, Y. Shimogaki, and Y. Nakano, *Appl. Phys. Lett.* **84**, 3703 (2004).

<sup>7</sup>I. Waki, C. Kumtornkittikul, Y. Shimogaki, and Y. Nakano, *Appl. Phys. Lett.* **82**, 4465 (2003).

<sup>8</sup>S. Nicolay, E. Feltin, J.-F. Carlin, M. Mosca, L. Nevou, M. Tchernencheva, F. H. Julien, M. Illegems, and N. Grandjean, *Appl. Phys. Lett.* **88**, 151902 (2006).

<sup>9</sup>J. Faist, F. Capasso, C. Sirtori, D. L. Sivco, A. L. Hutchinson, S. N. G. Chu, and A. Y. Cho, *Appl. Phys. Lett.* **65**, 94 (1994).

<sup>10</sup>M. Helm, *The Basic Physics of Intersubband Transitions*, Semiconductors and Semimetals, Vol. 62 (Academic, London, 2000).

<sup>11</sup>F. Bernardini and V. Fiorentini, *Phys. Rev. B* **57**, R9427 (1998).

<sup>12</sup>V. Ursaki, I. Tiginyanu, P. Ricci, A. Anedda, S. Hubbard, and D. Pavlidis, *J. Appl. Phys.* **94**, 3875 (2003).

<sup>13</sup>W. Liu and A. A. Balandin, *J. Appl. Phys.* **97**, 123705 (2005).

<sup>14</sup>G. Bastard, E. E. Mendez, L. L. Chang, and L. Esaki, *Phys. Rev. B* **28**, 3241 (1983).